Journal of Sea Research 83 (2013) 30–39

Contents lists available at ScienceDirect

Journal of Sea Research

journal homepage: www.elsevier.com/locate/seares

A comparison of primary production models in an area of high mesoscale variability (South Shetland Islands, Antarctica)

Cristina García-Muñoz [a,*], Ángel López-Urrutia [b], Luis M. Lubián [a], Carlos M. García [c], Santiago Hernández-León [d]

[a] Departamento de Ecología y Gestión costera, Instituto de Ciencias Marinas de Andalucía (ICMAN-CSIC), 11510 Puerto Real, Cádiz, Spain
[b] Centro Oceanográfico de Gijón, Instituto Español de Oceanografía, 33212 Gijón, Asturias, Spain
[c] Departamento de Biología, Facultad de Ciencias del Mar y Ambientales, Universidad de Cádiz, 11510 Puerto Real, Cádiz, Spain
[d] Institute of Oceanography and Global Change, Universidad de Las Palmas de Gran Canaria, 35017 Las Palmas de Gran Canaria, Islas Canarias, Spain

ARTICLE INFO

Article history:
Received 14 December 2012
Received in revised form 21 March 2013
Accepted 27 March 2013
Available online 17 April 2013

Keywords:
Primary production
Models
Mesoscale
Chlorophyll
Carbon
Nutrients

ABSTRACT

Three types of primary productivity (PP) models were evaluated in a mesoscale area around the South Shetland Islands (Antarctica). Input variables were: phytoplankton carbon biomass, Chlorophyll *a*, sea water temperature, daily irradiance, among others, collected in situ during an oceanographic cruise (*COUPLING*, January 2010). Models of the first type were based on Chl *a* measurements: the widely used model VGPM (Behrenfeld and Falkowski, 1997) and a derived version developed for the Western Antarctic Peninsula (Dierssen et al., 2000). The second type included two models based on phytoplankton carbon biomass: one developed for the whole Southern Ocean (Arrigo et al., 2008) and one based on the Metabolic Theory of Ecology developed by López-Urrutia et al. (2006), being the first time that a model with these features is used for Antarctic waters. The third type was an updated version of the carbon-based model CbPM (first described by Behrenfeld et al. (2005)) based on the Chl *a*/carbon biomass ratio modulation. The degree of agreement among the results between the different types of models turned out to be low (>30% of difference), but high within models of the same type (<10% of difference). Biomass-based model predictions differed the most from those estimated by the other two types. The differences in PP estimates were primarily attributed to the different ways these models treat the phytoplankton assemblage, along with the difference in input variables. Among the five models evaluated, the output from the modified version of the CbPM showed the lowest bias (0.55) being the most realistic. It made a special attempt to detect the factors controlling phytoplankton physiological state, showing a nutrient limitation towards the Drake area similar to the one observed for the in situ PP values.

1. Introduction

The determination of primary productivity (PP) and its spatial and temporal variability remains one of the major goals of biological oceanography (Barber and Hilting, 2002). Net primary production (NPP: mg C m^{-2} d^{-1}) is a key parameter in ecosystem research and carbon cycling (Behrenfeld et al., 2005). During the last decades, remote sensing models aiming to estimate ocean NPP have been developed in order to monitor large areas of the global ocean (i.e. Behrenfeld and Falkowski, 1997; Behrenfeld et al., 2005; Eppley et al., 1985; Marra et al., 2003; Westberry et al., 2008) as well as specific sites like the Southern Ocean (SO) (Arrigo et al., 2008; Dierssen et al., 2000). Several works have focused on the comparison of the results obtained by these models (Campbell et al., 2002; Carr et al., 2006) and controversial results were observed related to the algorithms used, especially for the Antarctic waters (Campbell et al., 2002; Carr et al., 2006; Shang et al., 2010).

The SO is a well known High Nutrient Low Chlorophyll (HNLC) area, and it is generally assumed to be controlled by the supply of micronutrients (especially iron) and light (Alderkamp et al., 2010; Boyd et al., 2010; Hewes et al., 2009; Vernet et al., 2012; inter alia). This bottom-up control suggests that the ecosystem is sensitive to changes in physical forcing that influence the light and nutrient environment experienced by phytoplankton (e.g. upwelling, mixed layer depth, sea ice) (Rintoul et al., 2012). On average, the SO is characterized by its abundant macronutrients coupled with only the modest rates of annual average NPP (Arrigo et al., 1998; Moore and Abbott, 2000). Despite the generally low phytoplankton abundance, intense phytoplankton blooms occasionally develop, making productivity in the SO highly variable both temporally and spatially (Arrigo et al., 2008). In situ measurements of PP obtained in the Drake Passage and Bransfield Strait during the last decades (El-Sayed, 1967; Holm-Hansen and Mitchell, 1991; Varela et al., 2002, inter alia) showed a wide range of spatial (decreasing PP values towards the Drake Passage) and seasonal

* Corresponding author at: Instituto de Ciencias Marinas de Andalucía (ICMAN-CSIC), Av. República Saharauii s/n, CP. 11510 Puerto Real, Cádiz, Spain.
E-mail address: cristina.garcia@icman.csic.es (C. García-Muñoz).

1385-1101/$ – see front matter
http://dx.doi.org/10.1016/j.seares.2013.03.015

variability, detecting strong differences between shelf and open water stations. Although the Bransfield Strait region reached high PP values during the austral summer (e.g. 1.2 g C m^{-2} d^{-1} in Holm-Hansen and Mitchell, 1991), these values are much lower than those reported for other Antarctic areas, especially in the Ross Sea (3.5 g C m^{-2} d^{-1}; in Smith and Gordon, 1997) and Amundsen Sea polynya (2.2 g C m^{-2} d^{-1}; in Lee et al., 2012). These in situ values are commonly measured using ^{14}C or ^{13}C incubations. Despite being widely used, some questions still remain about whether ^{14}C assimilation rates represent net or gross photosynthesis (or something in between) and whether the commonly employed manipulations yield biased results (Furnas, 2002; Li and Maestrini, 1993). Smith et al. (2000) suggested for their PP results on the Ross Sea that due to the nature of the irradiance field in the Antarctic, assemblages maintained in on-deck incubators received more light than those in situ, which resulted in photoinhibition. This in turn resulted in a 17% underestimate in on-deck productivity relative to in situ determinations. Using a modeling approach, Ross et al. (2011) found that the depth-integrated productivity from fixed-depth incubations tends to overestimate the net depth-integrated PP in natural conditions of a freely mixing water column by up to 25%. This overestimation can be turned into an underestimation of the same order of magnitude if the cells, in fact, become easily photoinhibited.

In this sense, the aim of this work was to compare different PP models developed for remote sensing data with in situ data in an Antarctic area characterized by high mesoscale variability. For this purpose, three types of remote-sensing models and one based in the Metabolic Theory of Ecology (MTE) were applied to in situ measurements obtained during *COUPLING* cruise (January 2010) around the South Shetland Islands (SSI).

Our objective was to test models with varying degrees of complexity, choosing those widely used and with input variables easily measurable in any oceanographic cruise. Among these algorithms, models based on Chlorophyll *a* (Chl *a*) measurements (Type 1) are the simplest: the Vertically Generalized Production Model (VGPM) proposed by Behrenfeld and Falkowski (1997) is probably one of the most widely used PP models. A version of VGPM derived for the western Antarctic Peninsula (wAP) by Dierssen et al. (2000) and recently used in this area (Vernet et al., 2012) was also evaluated. The second type of models, based on phytoplankton carbon biomass, was chosen, primarily, to compare if the results of a model developed exclusively for the SO (Arrigo et al., 2008) could be comparable with the output of a model based on the MTE (López-Urrutia et al., 2006), and thus validate whether the latter model could be useful for Antarctic waters. The third type of models under consideration is based on the use of the Chl *a*/carbon biomass (Chl *a*/C) ratio as a proxy to evaluate resource limitation. It was chosen because the limitation of summer time phytoplankton accumulation has been attributed to the low iron concentration towards the Drake Passage (Alderkamp et al., 2011; Hewes et al., 2009), while the Bransfield Strait has a relatively high iron concentration (Ardelan et al., 2010; Hewes et al., 2008). Laboratory experiments have long shown that phytoplankton response to changes in light, nutrients, and temperature conditions is well quantified by changes in the ratio of Chl *a* to C (e.g., Geider, 1987; MacIntyre et al., 2002; Sakshaug et al., 1989).

The results obtained with the different models were compared and discussed to discern why they differ. The previous knowledge of the study area has allowed us to implement improvements in the selected models in order to achieve realistic results of PP based on the limitation by light, also by a deepening of the mixed layer depth, and nutrient concentration.

2. Methods

2.1. Data sources

All the data used in this study were collected from *RV BIO-Hespérides* during *COUPLING* cruise, 8th to 27th January 2010. The survey was conducted around the SSI, with a main transect sampled from the Drake Passage to the Bransfield Strait (hereafter, Transect 1, Fig. 1). At each station vertical profiles of temperature, salinity and in situ fluorescence were obtained using a combined Conductivity–Temperature–Depth sensor (CTD) Seabird 911plus with a Seapoint fluorescence sensor attached to a rosette system of 24 oceanographic 12-L Niskin bottles. Maximum depths were down to near the bottom in coastal and shelf stations and down to 1000 m in offshore stations. Water sampling was performed at 6 fixed depths (5, 10, 25, 50, 75 and 100 m) including the depth of the fluorescence maximum (DFM) for plankton related variables (Chl *a*, phytoplankton abundance and individual size measurements) and at 10–11 depths (from 5 to 1000 m) for macronutrient analyses.

The Mixed Layer Depth (*MLD*) was inferred from temperature and salinity profiles using the algorithm by Kara et al. (2000). Surface solar irradiance was monitored on deck with a Kipp & Zonen CM11 sensor (285 to 2800 nm, spectral range). Daily photosynthetically active radiation (PAR, $\lambda = 400$–700 nm) at the surface was estimated as the sum of the average surface solar irradiance each hour (W m^{-2}), and a factor of 2.08 mol photons m^{-2} s^{-1} MW^{-1} (Ting and Giacomelli, 1987). Daily PAR just below the sea surface (Io) was estimated considering 0.8 as the transmittance at the air–sea interface (Austin, 1974). For each station a vertical light attenuation coefficient K_d (m^{-1}) was calculated by measuring the PAR values at 1 m depth intervals in the water column with a hemispherical quantum sensor (CI PAR, Chelsea instrument, Relative Spectral Sensitivity flat to ±3% from 450–700 nm). The euphotic zone depth (*Zeu*) was defined as the depth at which the light intensity was attenuated to 1% of the value just below the surface, and was calculated as $\ln(0.01)/K_d$.

Chlorophyll-*a* concentration was determined fluorometrically. Water samples (250-mL) were sequentially filtered through 20, 2 and 0.2 μm polycarbonate membrane filters and pigments were extracted in 90% acetone at −20 °C overnight. Fluorescence was measured on a Turner TD-700 fluorometer which had been calibrated with pure Chl *a* following the UNESCO (1994) standard protocol.

Aliquots for inorganic nutrient determination (nitrate and silicic acid) were collected in 5 mL polyethylene tubes. Samples were filtered through 0.45 μm (Minisart NY 25) and stored frozen (−80 °C) until analysis by means of a Technicon TRAACS 800 and Skalar San ++ System Autoanalyzers using standard protocols (Grasshoff et al., 1983). We used the Si* tracer (calculated as the concentration of silicic acid minus nitrate concentration), defined by Sarmiento et al. (2004), as a proxy for iron limitation in the sampling area.

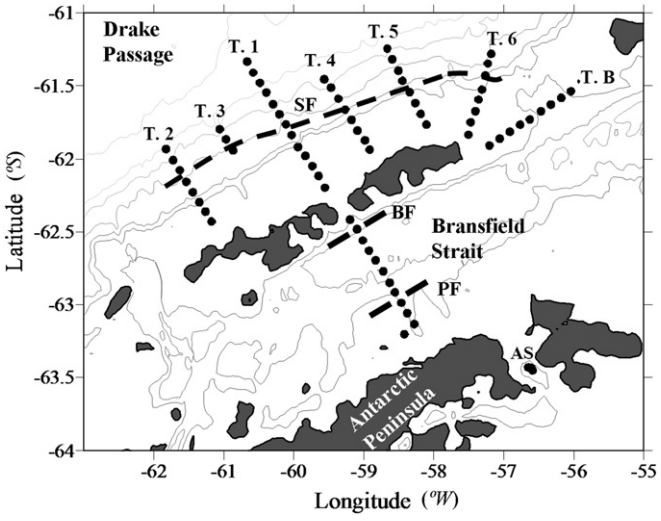

Fig. 1. Area of study and stations location. AS: Antarctic Sound, BF: Bransfield Front, PF: Peninsula Front, SF: Shetland Front. For further details of fronts' characteristics and location and surface currents see Sangrà et al. (2011) and Hewes et al. (2009).

Primary production was measured using the ^{13}C method (Hama et al., 1983) in a total of 11 stations at two sampling depths, including surface and the DFM. Water samples were transferred to 2 L polycarbonate bottles previously rinsed with 10% HCl and distilled–deionized water. After addition of $NaH^{13}CO_3$ at about 10% of total inorganic carbon in the ambient water, the samples were incubated for about 12 h in a tank on deck at in situ temperature with running surface seawater under light intensity regulated by meshes of different sizes to simulate water column conditions. Initial and final particulate organic carbon, and particulate material used for isotope analysis were filtered through GF/F filters. They were frozen and stored at −20 °C until analysis. Particulate organic carbon was measured using a CHN analyzer (Carlo Erba EA 1108) and isotopes in a mass spectrometer equipped with an elemental analyzer (Flash EA11 ThermoFinnigan with Deltaplus).

Phytoplankton composition and abundance were analyzed by overlapping Flow cytometry and FlowCAM techniques to include the whole phytoplankton assemblage from 2 to 200 μm Equivalent Spherical Diameter (ESD). Phototrophic prokaryotes in the picoplankton size range were not detected along the study area using flow cytometry. A detailed description of both techniques is presented elsewhere (García-Muñoz et al., in press). Plankton volume was converted to carbon units using the equations proposed by Menden-Deuer and Lessard (2000).

2.2. Models

Five different models were used to calculate integrated NPP (mg C m^{-2} d^{-1}) based on the data surveyed during the cruise. All symbols used were summarized in Table 1.

2.2.1. Type 1 — models based on Chl a

The original VGPM (Behrenfeld and Falkowski, 1997) and the derived version developed by Dierssen et al. (2000) with field data from the wAP, hereafter Dierssen model. Both models are not vertically resolved, in the sense that they estimate vertically integrated values from surface data.

In the VGPM, NPP was calculated as follows:

$$NPP\left(\text{mg C m}^{-2}\ \text{d}^{-1}\right) = Chl_0\ a \times Zeu \times f(Io) \times DL \times P^B opt \quad (1)$$

$$f(Io) = 0.66125 \times Io/(Io + 4.1) \quad (2)$$

where $P^B opt$ was defined as a function of sea surface temperature (SST),

$$P^B opt = -3.27 \times 10^{-8}T^7 + 3.4132 \times 10^{-6}T^6 - 1.348 \times 10^{-4}T^5 + 2.462 \times 10^{-3}T^4 - 0.0205 \times T^3 + 0.0617 \times T^2 + 0.2749 \times T + 1.2956. \quad (3)$$

In Dierssen's biooptical model NPP was a function of:

$$NPP\left(\text{mg C m}^{-2}\ \text{d}^{-1}\right) = Chl_0\ a \times Zeu \times F \times DL \times P^B opt \quad (4)$$

where F is the empirically estimated ratio of mean Chl a normalized productivity in the water column to $P^B opt$, calculated as:

$$F = Io/(Io + 11.77). \quad (5)$$

As Dierssen et al. (2000) did, we have parameterized the model using their $P^B opt$ median value (1.09 mg C mg Chl a^{-1} h^{-1}).

2.2.2. Type 2 — models based on phytoplankton carbon biomass

In this study, we have tested a model based on the MTE developed by López-Urrutia et al. (2006), hereafter MTE model, and a PP algorithm parameterized specifically for use in SO waters developed by Arrigo et al. (2008), hereafter Arrigo model. As far as we know, this is the first time that a model based on the MTE is used for the calculation of PP in Antarctic waters.

In the MTE model, PP was calculated as:

$$\ln\left(NPP\left(\text{mmol O}_2\text{cell}^{-1}\ \text{d}^{-1}\right)\right)_z = \ln Nc + \alpha \times \ln(M_i) - E_a \times (1/kT) + \ln(I_z/(I_z + K_m)) :$$
$$\ln\left(NPP\left(\text{mmol O}_2\text{cell}^{-1}\ \text{d}^{-1}\right)\right)_z = -11.56 + 1.02 \times \ln(M_i) - 0.28 \times (1/kT) + \ln(I_z/(I_z + 1.52)) \quad (6)$$

$$I_z = Io \times \exp(-K_d \times Z) \quad (7)$$

where Nc is the respective normalization constant, α is the allometric exponent, E_a is the activation energy and K_m is the Michaelis–Menten half-saturation constant. We used a photosynthetic quotient (PQ) of 1.25 for carbon conversion and summed the individual PP cell rate in each depth to obtain PP in mg C m^{-3} d^{-1}.

Arrigo model (modified from Arrigo et al., 1998) calculates the rate of PP (mg C m^{-3} h^{-1}) as a function of diurnal changes in spectral

Table 1
List of commonly used symbols throughout the text.

Symbol	Units	Data range	Description
$C_{(z)}$	mg C m^{-3}	32.90–278.95	Phytoplankton biomass at each depth
$Chl_0\ a$	mg m^{-3}	0.09–1.98	Surface Chlorophyll a concentration
Chl $a_{(z)}$	mg m^{-3}	0.04–2.39	Chlorophyll a concentration at each depth
DL	h	16	Length of day time
E_a	eV	0.28	Activation energy
F		0.41–0.81	Relationship of $P^B opt$ to the mean chl-normalized productivity
Io	mol photons m^{-2} d^{-1}	8.17–49.55	Surface daily photosynthetically available radiation (PAR)
I_{MLD}	mol photons m^{-2} d^{-1}	0.32–17.47	Median mixed layer daily PAR
I_z	mol photons m^{-2} d^{-1}	8.57×10^{-5} – 35.27	Daily PAR at each depth
k	eV K^{-1}	8.62×10^{-5}	Boltzmann's constant
K_d	m^{-1}	0.03–0.13	Diffusive attenuation coefficient
K_m	mol photons m^{-2} d^{-1}	1.52	Michaelis–Menten half-saturation constant
M_i	pg C $cell^{-1}$	$1.13–3.50 \times 10^5$	Individual phytoplankton biomass
MLD	m	14–267	Mixed layer depth
N_c		9.54×10^{-6}	Normalization constant
P^Bopt	mg C mg Chl^{-1} h^{-1}	1.09–1.88 (1.09 in Dierssen model)	Maximum chl-normalized C fixation rate within a water column
SST	°C	−1.11–1.76	Sea surface temperature
$T_{(z)}$	°C (°K in MTE model)	−1.14–1.76	Sea water temperature at each depth
Zeu	m	36–144	Euphotic zone depth
α		1.02	Allometric exponent
μ_0	d^{-1}	0.59	Phytoplankton growth rate at 0 °C, as in Eppley (1972)
$\mu_{(z)}$	d^{-1} (h^{-1} in Arrigo model)	0.01–0.59	Phytoplankton growth rate at each depth
μ_{max}	d^{-1}	0.55–0.66 (0.66 in CbPM model)	Maximun phytoplankton growth rate

downwelling irradiance, temperature and Chl *a* concentration. They assume that Chl *a* concentration is uniform within the upper mixed layer as well as a constant phytoplankton carbon to Chl *a* (C/Chl *a*) ratio (88.5 g:g) along the whole SO. However, this approach is too simplistic for a mesoscale range, therefore we modified the initial equation (Eq. (8)) to Eq. (9):

$$NPP\left(\text{mg C m}^{-2}\ \text{d}^{-1}\right) = \int_z \int_t \text{Chl } a_{(z)} \times \text{C/Chl } a \times \mu_{(z,t)}\ \text{dt dz} \tag{8}$$

$$NPP\left(\text{mg C m}^{-2}\ \text{d}^{-1}\right) = \int_z \int_t C_{(z)} \times \mu_{(z,t)} \text{dt dz} \tag{9}$$

where $\mu_{(z,t)}$ is the net biomass-specific growth rate (h^{-1}) at a given time t and depth z. $\mu_{(z,t)}$ is calculated as a product of the temperature dependent upper limit to net phytoplankton growth rate, μ_{max} (h^{-1}) and the irradiance limitation term, *L* (dimensionless). μ_{max} was calculated according to the equation:

$$\mu_{\max(z)} = \mu_0\ \exp\left(r \times T_{(z)}\right) \tag{10}$$

where μ_0 is the phytoplankton net growth rate at 0 °C (0.59 day^{-1}) and r is a rate constant (0.0633 $°C^{-1}$) that determines the sensitivity of μ_{max} to temperature, *T* (°C). *L*(*z*, *t*) was calculated for each depth and each time step following the Eqs. (10) to (14) in Arrigo et al. (2008).

Arrigo model is in essence very similar to MTE model, the main difference is that MTE calculates NPP on an individual basis while Arrigo uses the total biomass of the phytoplankton community.

2.2.3. Type 3 — a model based on the Chl a/C ratio

We have reviewed the original CbPM model (first described by Behrenfeld et al. (2005), and later updated by Westberry et al. (2008)) using our in situ Antarctic data. The primary processes which drive vertical changes in Chl *a* concentration in the CbPM are those associated with physiological, intracellular adjustments to ambient light and nutrient conditions:

$$NPP\left(\text{mg C m}^{-3}\ \text{d}^{-1}\right) = \mu_{(z)} \times C_{(z)} \tag{11}$$

$$\mu_{(z)} = \mu_{\max} \times f(Nut, T)_{(z)} \times f(Ig) \tag{12}$$

$$f(Nut, T)_{(z)} = (Chl\,a/C)_{in\ situ} / (Chl\,a/C)_{\max} \tag{13}$$

$$(Chl\,a/C)_{\max} = 0.022 + (0.045\text{–}0.022) \times \exp(-3 \times Ig) \tag{14}$$

$$f(Ig) = 1 - \exp(-3 \times Ig) \tag{15}$$

where, *f*(*Nut*, *T*) accounts for reductions in growth rate due to nutrient and temperature limitation (range: 0 to 1), *f*(*Ig*) accounts for reductions in growth rate due to light limitation (range: 0 to 1), and μ_{max} is the maximum potential community growth rate under optimal conditions calculated using Eppley's (1972) equation and the maximum temperature detected in the study area.

For those depths over the *MLD*, the irradiance term (*Ig*) was calculated as the median mixed layer light level (I_{MLD}), following Eq. (2) in Figueiras et al. (1999), as:

$$I_{MLD} = \sum (Io \times \exp(-K_d \times Z))/MLD \tag{16}$$

while for depths below the *MLD*, *Ig* was calculated with the respective I_z, as suggested by Westberry et al. (2008).

Eq. (14) represents Chl *a*/C in nutrient-replete, optimal growth conditions for a large sum of regions; therefore we re-parameterize this equation using quantile regression, enveloping 95% of our in situ data.

For both type 2 and 3 models we performed trapezoidal integrations. The integration depth was that of the *Zeu* or the *MLD* whichever was deeper at each station.

To evaluate the differences and compare between the model outputs we have calculated the percentage of difference as:

$$\%\ difference = ((Log\ \ Model_2 - Log\ \ Model_1)/Log\ Model_1) \times 100. \tag{17}$$

To evaluate the fitness of a model, we can distinguish between an uncertainty component stemming from model imperfection and a component originating from an inexact knowledge of input values.

There is no way to discern whether an input parameter or variable measured in situ was better sampled, analyzed or calculated than other. Therefore we decided to assume that this latter source of error was constant for all the models evaluated and influence equally to the results, being the model imperfection which really controls the fitness.

To quantify uncertainty in the NPP output of the vertically resolved models, we followed Milutinović and Bertino (2011) and compared modeled values with a coincident observed measurement which served as reference, by finding a logarithmic difference (δ^{LOG}). The zero centered root mean square ($RMSD_0^{LOG}$) was used as a measure of the portion of uncertainty associated with the natural variability:

$$\delta^{LOG} = Log(Mod) - Log(Obs) \tag{19}$$

$$RMSD_0^{LOG} = \sqrt{1/(N-1)\sum_{i=1}^{N}\left(\delta_i^{LOG} - B^{LOG}\right)^2} \tag{20}$$

$$B^{LOG} = \overline{\delta^{LOG}} = 1/N\sum_{i=1}^{N}(Log(Mod_i) - Log(Obs_i)) \tag{21}$$

where B^{LOG} represents the respective value of bias, i.e. the mean discrepancy between modeled and observed values.

3. Results

3.1. Input variables

Sea water temperature varied from −1.14 to 1.76 °C, reaching the highest temperatures in the northern stations of the Drake area related to the Antarctic Surface Water (AASW) (Fig. 2a), and the lowest south of the Peninsula Front (PF, sensu Sangrà et al., 2011, Fig. 1) towards the Antarctic Peninsula influenced by the Transitional Weddell Water (TWW) (Fig. 2d).

The *MLD* was modulated by the presence of hydrographical fronts and subduction zones (Sangrà et al., 2012), reaching the lowest values (<20 m) in the northern SSI shelf and the PF. The highest values (up to 267 m) were recorded in the Antarctic Sound (AS).

Irradiance at high latitude is influenced by the height of the sun over the horizon. During the cruise summer day length was on average 16 h. Surface daily PAR ranged between 8 and 50 mol photons $m^{-2}\ d^{-1}$, with the highest values recorded at stations sampled within the first part of the cruise (January 8th to 11th) in the central Bransfield Strait. The calculated diffuse attenuation coefficient for downwelling PAR (K_d) ranged from 0.03 m^{-1} (in the Drake area) to 0.13 m^{-1} (in the AS); thereby *Zeu* reached the deepest values, >50 m depth, towards the Drake area (Fig. 2a), while the shallowest *Zeu* were detected close to the SSI (<50 m depth) (Fig. 2b) and in the AS. Levels of total daily PAR in the upper mixed layer (I_{MLD}) were the highest at the hydrographical fronts in the Bransfield Strait (14–17.5 mol photons $m^{-2}\ d^{-1}$) due to the shallowing of the *MLD*, and in the Drake area due to low K_d detected (Fig. 3a).

Chl *a* concentration ranged between 0.04 and 2.39 mg m^{-3}. It was very low (<0.4 mg m^{-3}) in the upper mixed layer (down to 50 m) in

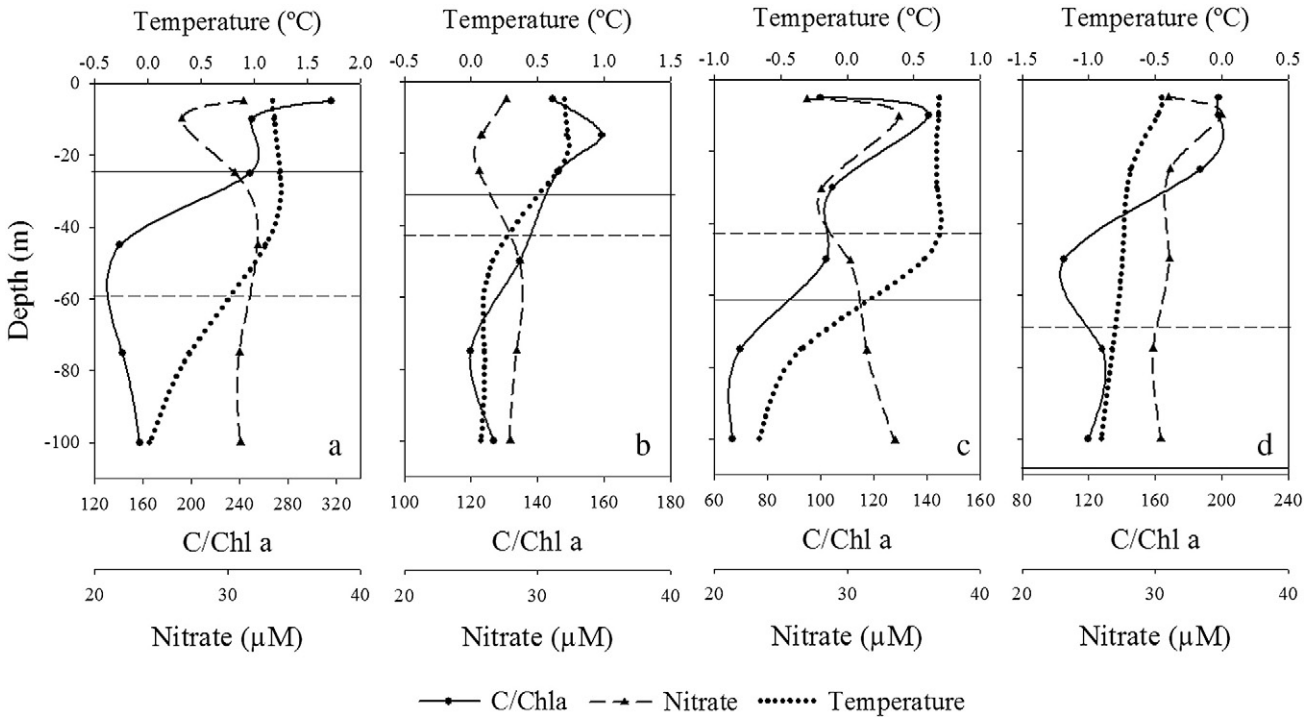

Fig. 2. Vertical profiles of temperature (°C), nitrate concentration (μM) and C/Chl *a* ratios (mg:mg) at selected stations in the Drake area (a), the SSI shelf (b), the Bransfield Strait between BF and PF (c) and south of the PF (d). Solid horizontal line represents the *MLD* and dashed line the *Zeu*.

the northern part of T.1, T.2, T.4, T.5 and T.6, corresponding to the AASW (Teira et al., 2012), but increased towards the southern part of T.1 and the AS. Surface concentrations (Fig. 3b) had the same distribution trend as integrated values ($r = 0.77$, $p < 0.05$, $N = 48$), with a strong contribution of phytoplankton under 20 μm ESD, along the study area (on average, 84% of total Chl *a*), except for the AS where microplanktonic size range (>20 μm ESD) predominated (up to 85% of total Chl *a*).

Nitrate concentrations were almost constant across the sampling stations and along the water column (30.41 ± 5.27 μM, $N = 526$). Although the highest variability was reached in the upper layer (from surface to 100 m), we did not observe levels to decrease to values that could limit phytoplankton production (Smayda, 1997 and references therein) (Fig. 2). Silicic acid concentrations showed a wide range of values throughout the vertical profiles between 15.60 μM in surface waters and 108.88 μM in the near-bottom waters. A spatial variability was also detected in the upper layer reaching the lowest values towards the Drake area (data not shown). This latter area has been hypothesized to be limited by low dissolved iron concentrations (Holm-Hansen et al., 2005), therefore the Si* tracer (Sarmiento et al., 2004) was selected as a reference to detect this limitation. Si* ratio followed the same trend as the silicic acid concentration ($r = 0.95$, $p < 0.05$, $N = 526$) increasing from surface to bottom waters (from −10.96 to 87.78) and from the Bransfield Strait to the Drake area (Fig. 4). The pattern in the northern half of Fig. 4 was consistent with those observed along the rest of the northern transects (T.2–T.6).

PP ^{13}C values ranged from 0.52 to 19.32 mg C m^{-3} d^{-1}. Despite the paucity of samples, only 11 stations sampled, an overall trend was detected. PP values were lower (<5 mg C m^{-3} d^{-1}) in surface waters at those stations located in the northern part of the Drake area (Teira et al., 2012).

Phytoplankton carbon biomass derived from cell counts and volume/biomass conversions (Menden-Deuer and Lessard, 2000), from 2 to 200 μm ESD, varied widely in each sampling depth between 32.90 and 278.95 mg C m^{-3}. The highest biomass concentrations (over 200 mg C m^{-3}) were detected in surface waters of the northern SSI shelf and the fronts located in the Bransfield Strait (Fig. 3c) while the lowest concentrations were detected in the deeper sampling depths, around 100 m, except for those stations with deep *MLD* whose biomass values were low but homogeneous along the water column. C/Chl *a* ratios calculated using phytoplankton carbon biomass values varied widely across the sampling sites and depths reaching minimum values (30–50 mg:mg) in the Bransfield Strait (ca. 100 m) (Fig. 2c) and ratios over 300 (mg:mg) in surface waters of the Drake area (Fig. 2a).

3.2. Comparison among models results

The mean value of NPP calculated from MTE and Arrigo were the highest, and varied widely across the stations (2531 ± 1068 mg C m^{-2} d^{-1}, 1447 ± 502 mg C m^{-2} d^{-1}, respectively). NPP values from VGPM and Dierssen were the lowest (685 ± 301 mg C m^{-2} d^{-1}, 601 ± 301 mg C m^{-2} d^{-1}, respectively), whereas median values were obtained by the modified version of CbPM (776 ± 481 mg C m^{-2} d^{-1}) (Table 2).

The production estimated from ocean-color algorithms based on Chl *a* (Type 1) was found to be highly correlated between them when using in situ data as the inputs of the algorithms, with a slope close to a 1:1 relationship (Fig. 5a). The determination of $P^B opt$ or maximum photosynthetic rate in the water column is a key parameter in these models. Dierssen et al. (2000) suggested that VGPM tends to overestimate $P^B opt$ for the temperatures between 0 and 2 °C and varies by a factor of seven within their temperature range. In our case $P^B opt$, calculated using the SST approach of Behrenfeld and Falkowski (1997), ranged between 1.09 and 1.88 mg C mg Chl^{-1} h^{-1}, values close to the median used by Dierssen model (1.09 mg C mg Chl^{-1} h^{-1}). A priori, this might indicate that the physiological state of phytoplankton in this area is strongly affected by temperature.

Biomass-based models (Type 2) gave significantly higher NPP results than Type 1 models (*t*-test, $p < 0.05$). Although MTE and Arrigo showed strong correlations (Fig. 4b, $R^2 = 0.923$), the results returned by MTE nearly doubled those of Arrigo. The irradiance limitation terms of both models behave similarly tending to zero as the irradiance decreases with depth. Cell daily production (mmol O_2 $cell^{-1}$ d^{-1}) in the MTE model ranged between 3.931×10^{-12} and 1.621×10^{-5}

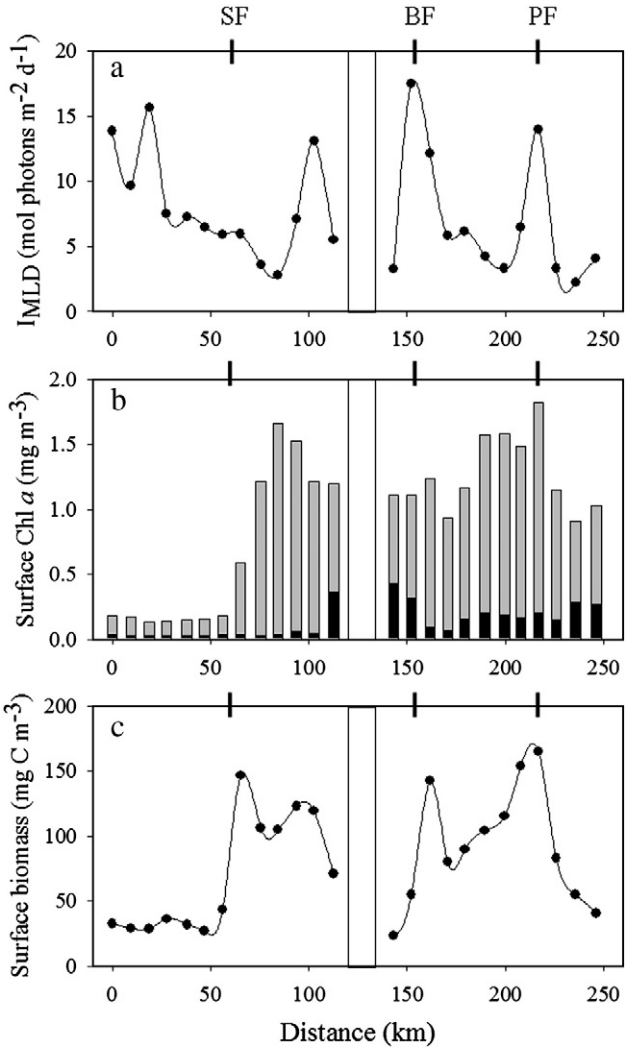

Fig. 3. I_{MLD} (a), surface Chl *a* concentration (mg m^{-3}) (gray bars represented Chl *a* < 20 μm ESD and black bars Chl *a* > 20 μm ESD) (b) and surface phytoplankton biomass (mg C m^{-3}) (c) along Transect 1, north (left) to south (right). Mesoscale fronts detected across the transect are located above the figure. BF: Bransfield Front, PF: Peninsula Front, SF: Shetland Front.

values corresponding to cell size close to 2 μm and 200 μm ESD, respectively. These values are within the range of those compiled by López-Urrutia et al. (2006) (see their Table 3, which is published as supporting information). This latter model was developed for a wide range of temperatures (0–30 °C) but few data close to 0 °C and none negative were included in the original database.

Table 2
Mean and standard deviation (SD) of the NPP output (mg C m^{-2} d^{-1}) of the different models used and the summary of uncertainties in NPP (mg C m^{-3} d^{-1}) measurements between observed and modeled values (N − 16).

	VGPM N = 53	Dierssen N = 53	MTE N = 45	Arrigo N = 45	CbPM N = 45
Mean ± SD	684.6 ± 300.9	601.1 ± 300.6	2531.3 ± 1068.3	1446.6 ± 501.9	775.9 ± 480.8
Output	Component of output uncertainty				
NPP (mg C m^{-3} d^{-1})	Bias		1.14	0.87	0.55
	Zero-centered RMSD		1.75	1.45	1.21

In the case of the modified CbPM model (Type 3), significant differences (*t*-test, $p < 0.05$) were found among average Chl *a*/C ratios of low (<1 mg Chl *a* m^{-3}) and high biomass communities (>1 mg Chl *a* m^{-3}), with values close to 0.005 and 0.010 mg C mg Chl a^{-1}, respectively. The new equation obtained for the $(\text{Chl } a/\text{C})_{max}$ ratio after the re-parameterization was:

$$(\text{Chl } a/\text{C})_{max} = 0.0091 + 0.0079 \times \exp(-3 \times Ig). \quad (22)$$

This model returned the highest values (>1000 mg C m^{-2} d^{-1}) for coastal stations of T.1, T.6 and T.B. and along the Bransfield Strait, where values of up to 2000 mg C m^{-2} d^{-1} were reached (Fig. 6).

The highest percentage of difference for each pair of models was detected between Type 1 and 2 for those stations located in the Drake area (30–40%). The integrated NPP values of the modified CbPM model were close to Type 1 results, except at those stations north of SF and the AS, where the lowest Chl *a* values and the highest *MLD* were detected, respectively (Fig. 7). The overall trend in the study area was well defined between the 2nd and 3rd Type models with a power equation: $\ln Y = \ln a + b \ln X \Rightarrow Y = a X^b$: $NPP\ Arrigo = 2.756 \times (NPP\ CbPM)^{0.893}$ ($R^2 = 0.957$) (Fig. 8). CbPM vs. MTE gave similar results (data not shown).

The lowest mean discrepancy (bias) and standard deviation (Zero-centered RMSD) between modeled and observed data were detected for the modified CbPM model (Table 2).

4. Discussion

The general conclusion obtained by those authors who estimate and compare PP using general models for areas as heterogeneous as the whole SO, is the introduction of large errors (either overestimates or

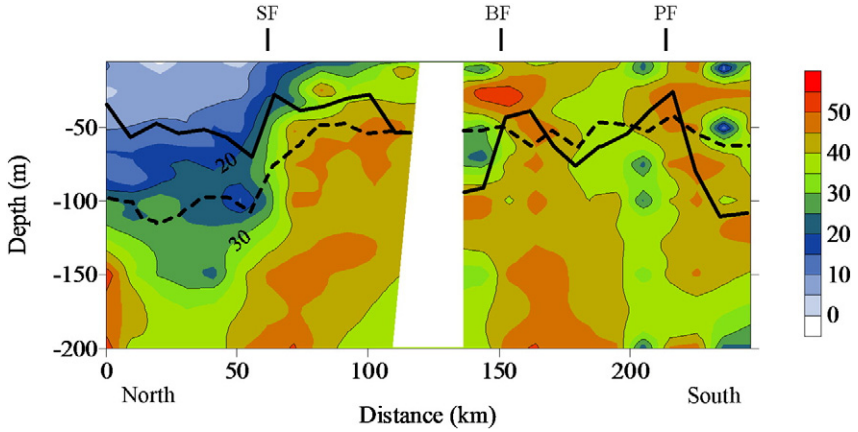

Fig. 4. Si* distribution along Transect 1, north (left) to south (right). Thick line represents the *MLD* and dashed line the *Zeu*. Mesoscale fronts detected across the transect are located above the figure. BF: Bransfield Front, PF: Peninsula Front, SF: Shetland Front.

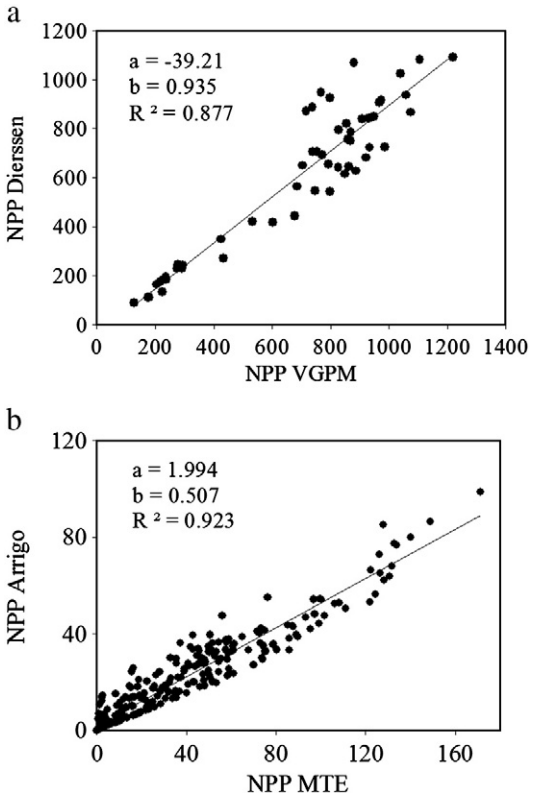

Fig. 5. Linear regression between (a) integrated models based on Chl *a* (VGPM vs. Dierssen, mg C m^{-2} d^{-1}, N = 53) and (b) discrete depths models based on phytoplankton biomass (MTE vs. Arrigo, mg C m^{-3} d^{-1}, N = 253).

underestimates) due to the lack of punctual information (hydrographical features, nutrients, community structure) (Carr et al., 2006). Success, then, will be measured by a more complete view of the abundance and distribution of primary producers and by increased understanding of fundamental processes governing marine ecosystems (Vernet and Smith, 2007). It is necessary to establish boundary conditions to obtain good results, especially at a mesoscale range. Carr et al. (2006) affirmed that the SO is unquestionably the most challenging large basin. Among

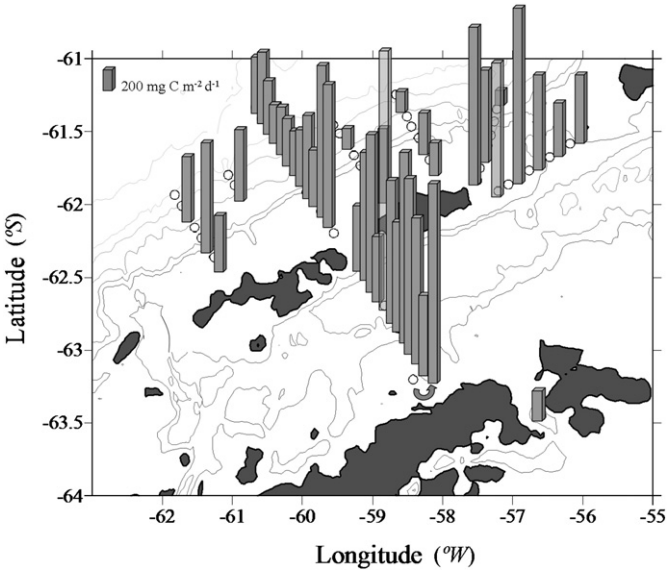

Fig. 6. Net Primary Production (NPP: mg C m^{-2} d^{-1}) output from the modified CbPM model along the study area.

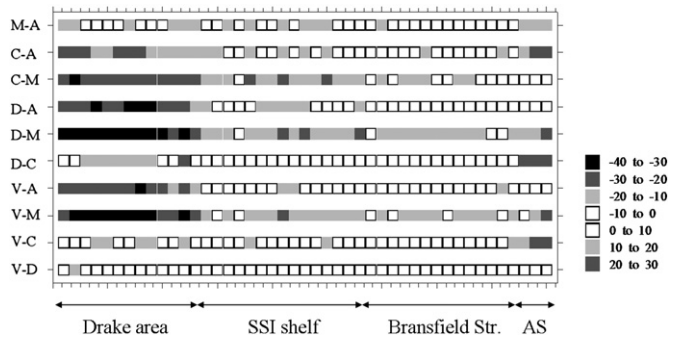

Fig. 7. % of difference between models' output (NPP: mg C m^{-2} d^{-1}) across the study area. A: Arrigo, C: CbPM, D: Dierssen, M: MTE, V: VGPM.

the 31 models used by Carr et al. (2006), the large divergence was attributed primarily to the differences in the way they formulated PP as a function of temperature. As a result, the extremely low temperatures characteristic of many SO waters (<0 °C) resulted in estimates of PP that varied over a range of 372% (Arrigo et al., 2008).

It has been found that vertically integrated models such as those based just in surface Chl *a* (Type 1, VGPM and derivatives) are too simple for a mesoscale area. Dierssen et al. (2000) compared their modeled results with in situ PP data measured along the wAP region using the ^{14}C method, obtaining high correlations that explained over 70% of the production variability. The variability not explained by the model could be due to the potential role of nutrients, especially iron, in controlling the distribution, timing, and rates of PP in the offshore stations of this region as suggested by Huang et al. (2012). Recently, Vernet et al. (2012) have used the Dierssen model, with vertically resolved field data. Although the model did not include a light limitation term for each sampling depth, they obtained satisfactory results throughout the austral fall in coastal sites of the wAP region. Our models' output revealed that the vertically integrated Dierssen model, as well as VGPM, could be useful for coastal stations around the SSI, where Chl *a* values are relatively high as well as dissolved iron concentrations (de Jong et al., 2012) and with no light limitation due to vertical structures such as subduction points (Fig. 7).

Type 2 models seem to overestimate the NPP rates along the study area. Prior studies have already reported modeled and in situ summer PP values over 2 g C m^{-2} d^{-1} around the SSI (Figueiras et al., 1999 and Lorenzo et al., 2002, respectively) but the comparison between the models' output, especially in the northern stations, revealed a strong divergence in this area. *COUPLING* cruise was conducted at the end of the phytoplankton bloom but in some stations the biomass, especially in the nanophytoplankton size range, was still high (Fig. 3b,c). As Type 2 models are based on irradiance, temperature, mixing process and body mass of phytoplankton without including any term for nutrient

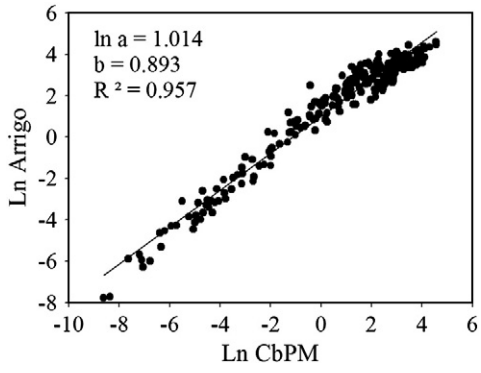

Fig. 8. Relationship between CbPM and Arrigo models (mg C m^{-3} d^{-1}, N = 253).

limitation, the high biomass values found in several stations exert a strong control in the output of the models, assuming that all the available biomass has the same production efficiency.

In those sampling sites situated in the Drake area, where the ice melting occurred much earlier in time and, hence, the seasonal phytoplankton bloom, a bulk of small-sized phytoplankton cells (2.8 ± 0.2 μm ESD) remained in subsurface waters reaching abundance values of up to 4600 cells mL^{-1}. Nevertheless, they did not achieve an optimal production yield with C/Chl *a* ratios over 200 mg C mg Chl^{-1} (Fig. 2) probably due to an iron limitation (Fig. 4). Therefore, the inclusion of only the phytoplankton biomass values in the models is not sufficient. Arrigo's theoretical model is simple in some assumptions because it uses constant ratios of C/Chl *a* for the whole SO and assumes that Chl *a* concentration is constant from surface to *MLD*. However, our input data do not confirm these assumptions. Therefore, it is necessary to introduce a variable C/Chl *a* ratio for each sampling depth (Fig. 2) as well as to evaluate which physicochemical characteristics drive this variation. On the other hand, the high correlation found between MTE and Arrigo's models highlights the potential uses of MTE in the SO, making suitable the 3/4 allometric scaling theory in this area with an activation energy for autotrophic processes ($E_a = 0.28$ eV) close to the reference value of $E_a = 0.32$ eV. Despite the similarity between Arrigo and MTE models, the main difference between the two approaches is that MTE calculates PP for each individual cell and then sums the PP of each cell to yield total PP, while Arrigo calculates PP directly using community biomass. This difference causes MTE PP estimates to be significantly higher, (*t*-test, $p < 0.05$), than those obtained by Arrigo.

Differences in the intercept, ln Nc, reflect large (over an order of magnitude), well-known size-independent taxonomic differences in metabolic rate (Irwin et al., 2006; Moloney and Field, 1989). It could be possible that MTE was overestimating nanophytoplankton production due to the predominance of small diatoms (García-Muñoz et al., in press). We suggest that it would be necessary to reconfigure the initial López-Urrutia et al.'s (2006) equation including production rates of phytoplankton cells at negative temperatures, as well as taking into account if a specific taxonomic group dominates in the study area, as Finkel et al. (2010) and Barnes et al. (2011) suggested. The novelty of MTE is not to report the existence of body-size or temperature dependence of metabolic rate, which have been known for over a century (López-Urrutia, 2008). The real challenge of MTE is that it provides framework to scale the effects of temperature, body size, and resources from the level of individual physiology to the ecology of populations, communities, and ecosystems (Brown et al., 2004), even for polar regions as Holding et al. (2011) demonstrate for the Arctic.

The original CbPM model (Type 3) described by Behrenfeld et al. (2005) states that, at a global scale, surface nutrients decrease with increasing SST. As nutrients cannot be directly measured from space, this model used SST to infer nutrient limitation from the term: $f(Nut, T) = (\text{Chl } a/C)_{\text{in situ}}/(\text{Chl } a/C)_{\max}$. When we modified the original model (see Methods section) and introduced the surveyed in situ nutrient data, a common trend between $f(Nut, T)$ and the Si* tracer was detected (Fig. 9a). The power relationship found between CbPM and Arrigo model (Fig. 8) showed that differences were more pronounced in those northern stations with PP values below 20 mg C m^{-3} d^{-1}, which agrees with our conclusion of the overestimation of Type 2 models in those stations limited by iron. Bio-available iron input into the Antarctic Peninsula-Bransfield Strait region is important for supporting high rates of PP in the SSI archipelago (Ardelan et al., 2010). It is well known that phytoplankton biomass (and hence Chl *a* levels) are iron-limited in the Drake Passage waters (Helbling et al., 1991; Hopkinson et al., 2007; Martin, 1990). Although few stations were sampled for $PP_{in\ situ}$ experiments, and the scarce values at discrete depths are not comparable to those of integrated models, a similar spatial trend with the Si* tracer was detected (Fig. 9b) showing significant positive correlations (Teira et al, 2012). This common trend with the Si* tracer was just obtained using the modified CbPM model.

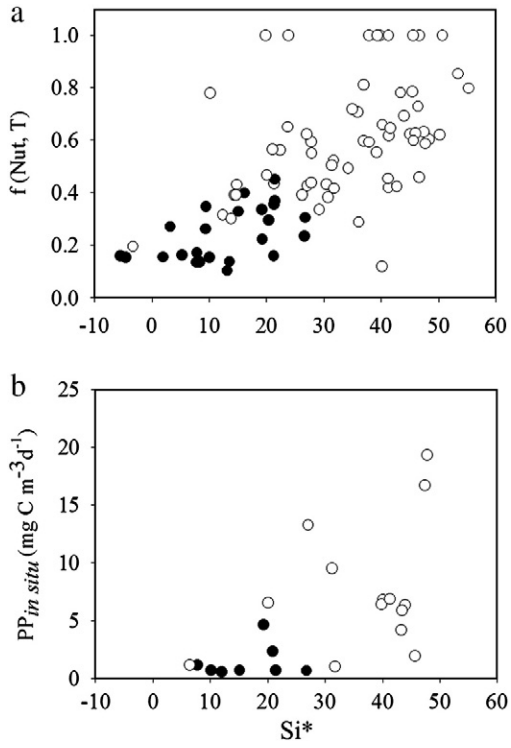

Fig. 9. Scatter plot between (a) Si* tracer and $f(Nut, T)$ and (b) Si* tracer and $PP_{in\ situ}$ (mg C m^{-3} d^{-1}). Colored dots are those stations situated in the Drake area.

Furthermore the lowest bias and standard deviation between modeled and observed PP values was detected for the updated CbPM model (Table 2). Notably, the Chl *a*/C-based estimates, when compared with the chlorophyll-based estimates, provide a different perspective on how ocean productivity is distributed over space and time (Vernet and Smith, 2007).

We did not include Westberry et al. (2008) nitracline depth consideration because nitrate was not limiting, taking constant values along the study area (Fig. 2). We neither considered their constant value of Chl *a*/C = 0.0003 (mg:mg) when $\mu = 0$, since the variation in results was negligible. Finally, taking into account the photosynthetic efficiency data obtained using a Fast Repetition Rate Fluorometer (FRRF) during the cruise, we observed photosaturation at surface layers in those stations sampled during sunny days (García-Muñoz et al., submitted for publication-b) and only stations with deep *MLD*s or sampled on very cloudy days were light limited. Therefore, the update introduced by Westberry et al. (2008) in the irradiance term, $f(Ig) = 1 - \exp(-5 \times Ig)$, was rejected for being less restrictive than Behrenfeld's original one and, thus, less accurate for our study area. Other improvements we introduced in the CbPM model have already been described in previous models as the original of Howard and Yoder (1997): the calculation of the maximum growth rate as a function of temperature according to Eppley (1972) and the integration of NPP to the *MLD* rather than to the *Zeu*, when *Zeu* was shallower than the *MLD*. In short, we consider that the results obtained with our modified version of CbPM (Fig. 5) were the most realistic and agree with the physicochemical and biological scenario that was taking place during the austral summer of 2010, coinciding with PP values obtained by prior field studies (from 423 to 3913 mg C m^{-2} d^{-1} in Basterretxea and Aristegui, 1999; 1110 ± 680 mg C m^{-2} d^{-1} in Lorenzo et al., 2002; 900 ± 200 mg C m^{-2} d^{-1} in Varela et al., 2002). This conclusion could be extrapolated to other sites of the SO, keeping in mind that each area of Antarctica is going to be limited by a specific variable; thus prior knowledge of physicochemical conditions along the study area is essential, especially for mesoscale studies.

In this paper we have highlighted the ability of models developed from remote sensing data to calculate PP with in situ data. PP can be satisfactorily estimated through these indirect methods and avoid the tedious ^{14}C or ^{13}C incubations on board. Among the five models used, the output from the modified version of the CbPM was the most realistic for its special feature to detect the factors that control the physiological state of phytoplankton, identifying a nutrient limitation towards the Drake area as the in situ measured PP values (Fig. 9). Finally, a model based on the MTE has been used to estimate PP rates in Antarctic waters. The results obtained differed greatly from those obtained in the other models, as it tends to overestimate NPP. A reconfiguration of the initial formulation to include production rates of phytoplankton cells at negative temperatures in the original database, as well as taking into account if a specific taxonomic group dominates in the study area, has been suggested.

Acknowledgments

We are grateful to the captain, crew, and scientists on board the R.V. Hespérides for their co-operation and logistic support during the cruise. Thanks are also given to Beatriz Mouriño and María Pérez for providing Chlorophyll *a* data, to María Lidia Nieves for providing primary production data, and to Eduardo Ramírez for his assistance in analyzing plankton samples. We also thank two anonymous reviewers for their valuable comments on a previous version of this manuscript. This work was supported by the CTM2008-06343-C02-02/ANT project from the Spanish Ministry of Science and Education. C.G-M.'s work was supported by a predoctoral fellowship from the Spanish Council for Research (CSIC), JAE-Predoc 2009. The work of A.L-U was supported by the CTM2009-13882/MAR project from the Spanish Ministry of Science and Education.

References

Alderkamp, A.-C., de Baar, H.J.W., Visser, R.J.W., Arrigo, K.R., 2010. Can photoinhibition control phytoplankton abundance in deeply mixed water columns of the Southern Ocean? Limnology and Oceanography 55, 1248–1264.

Alderkamp, A.-C., Garcon, V., de Baar, H.J.W., Arrigo, K.R., 2011. Short-term photoacclimation effects on photoinhibition of phytoplankton in the Drake Passage (Southern Ocean). Deep-Sea Research Part I 58, 943–955.

Ardelan, M.V., Holm-Hansen, O., Hewes, C.D., Reiss, C.S., Silva, N.S., Dulaiova, H., Steinnes, E., Sakshaug, E., 2010. Natural iron enrichment around the Antarctic Peninsula in the Southern Ocean. Biogeosciences 7, 11–25.

Arrigo, K.R., Worthen, D.L., Schnell, A., Lizotte, M.P., 1998. Primary production in Southern Ocean waters. Journal of Geophysical Research 103, 15587–15600.

Arrigo, K.R., van Dijken, G.L., Bushinsky, S., 2008. Primary production in the Southern Ocean, 1997—2006. Journal of Geophysical Research 113. http://dx.doi.org/10.1029/2007JC004551.

Austin, R.W., 1974. Inherent spectral radiance signatures of the ocean surface. In: Duntley, S.W., Austin, R.W., Wilson, W.H., Edgerton, C.F., Moran, S.E. (Eds.), Ocean color analysis. SIO reference 74–10. University of California, San Diego, pp. 1–20.

Barber, R., Hilting, A., 2002. History of the study of plankton productivity. In: Willams, P., Thomas, D., Reynolds, C. (Eds.), Phytoplankton Productivity: Carbon Assimilation in Marine and Freshwater Ecosystems. Blackwell, Oxford, pp. 16–43.

Barnes, C., Irigoien, X., Oliveira, J.A., Maxwell, D., Jennings, S., 2011. Predicting marine phytoplankton community size structure from empirical relationships with remotely sensed variables. Journal of Plankton Research 33, 13–24.

Basterretxea, G., Aristegui, J., 1999. Phytoplankton biomass and production during late austral spring (1991) and summer (1993) in the Bransfield Strait. Polar Biology 21, 11–22.

Behrenfeld, M.J., Falkowski, P.G., 1997. Photosynthetic rates derived from satellite-based chlorophyll concentration. Limnology and Oceanography 42, 1–20.

Behrenfeld, M.J., Boss, E., Siegel, D.A., Shea, D.M., 2005. Carbon-based ocean productivity and phytoplankton physiology from space. Global Biogeochemical Cycles 19. http://dx.doi.org/10.1029/2004GB002299.

Boyd, P.W., Strzepek, R., Fu, F., Hutchins, D.A., 2010. Environmental control of open-ocean phytoplankton groups: now and in the future. Limnology and Oceanography 55, 1353–1376.

Brown, J.H., Gillooly, J.F., Allen, A.P., Savage, V.M., West, G.B., 2004. Toward a metabolic theory of ecology. Ecology 85, 1771–1789.

Campbell, J., et al., 2002. Comparison of algorithms for estimating ocean primary production from surface chlorophyll, temperature, and irradiance. Global Biogeochemical Cycles 16. http://dx.doi.org/10.1029/2002GL015068.

Carr, M.-E., et al., 2006. A comparison of global estimates of marine primary production from ocean color. Deep-Sea Research Part II 53, 741–770.

de Jong, J., Schoemann, V., Lannuzel, D., Croot, P., de Baar, H., Tison, J.-L., 2012. Natural iron fertilization of the Atlantic sector of the Southern Ocean by continental shelf sources of the Antarctic Peninsula. Journal of Geophysical Research 117. http://dx.doi.org/10.1029/2011JG001679.

Dierssen, H.M., Vernet, M., Smith, R.C., 2000. Optimizing models for remotely estimating primary production in Antarctic coastal waters. Antarctic Science 12, 20–32.

El-Sayed, S.Z., 1967. On the productivity of the southwest Atlantic Ocean and the waters west of the Antarctic Peninsula. In: Schmitt, W., Llano, G. (Eds.), Biology of Antarctic seas III. Antarct. Res. Ser. 11. American Geophysical Union, Washington, D.C., pp. 15–47.

Eppley, R.W., 1972. Temperature and phytoplankton growth in the sea. Fish B-NOAA 70, 1063–1085.

Eppley, R.W., Stewart, E., Abbott, M.R., Heyman, U., 1985. Estimating ocean primary production from satellite chlorophyll. Introduction to regional differences and statistics for the Southern California Bight. Journal of Plankton Research 7, 57–70.

Figueiras, F.G., Arbones, B., Estrada, M., 1999. Implications of bio-optical modelling of phytoplankton photosynthesis in Antarctic waters: further evidence of no light limitation in the Bransfield Strait. Limnology and Oceanography 44, 1599–1608.

Finkel, Z.V., Beardall, J., Flynn, K.J., Quigg, A., Rees, T.A., Raven, J.A., 2010. Phytoplankton in a changing world: cell size and elemental stoichiometry. Journal of Plankton Research 32, 119–137.

Furnas, M.J., 2002. Measuring the growth rates of phytoplankton in natural populations. In: Rao, D.V.S., Rao, S., Ganapati, P.N., Lafond, E.C., Humphrey, G.F. (Eds.), Pelagic Ecology Methodology. CRC Press, Boca Raton, FL.

García-Muñoz, C., Lubián, L.M., García, C.M., Marrero-Díaz, A., Vernet, M., Sangrà, P., 2013. A mesoscale study of phytoplankton assemblages around the South Shetland Islands (Antarctic). Polar Biology (in press).

García-Muñoz, C., Sobrino, C., Lubián, L.M., García, C.M., Martínez-García, S., Sangrà, P., 2013. Factors controlling phytoplankton physiological state, abundance and structure around the South Shetland Islands (Antarctic). Marine Ecology Progress Series (submitted for publication).

Geider, R.J., 1987. Light and temperature dependence of the carbon to chlorophyll ratio in microalgae and cyanobacteria: implications for physiology and growth of phytoplankton. New Phytologist 106, 1–34.

Grasshoff, K., Ehrhardt, M., Kremling, K., 1983. Methods of Seawater Analysis. Verlag Chemie, Weinheim.

Hama, T., Miyazaki, T., Ogawa, Y., Iwakuma, T., Takahashi, M., Otsuki, A., Ichimura, S., 1983. Measurement of photosynthetic production of a marine phytoplankton population using a stable ^{13}C isotope. Marine Biology 73, 31–36.

Helbling, E.W., Villafañe, V., Holm-Hansen, O., 1991. Effect of iron on productivity and size distribution of Antarctic phytoplankton. Limnology and Oceanography 36, 1879–1885.

Hewes, C.D., Reiss, C.S., Kahru, M., Mitchell, B.G., Holm-Hansen, O., 2008. Control of phytoplankton biomass by dilution and mixing depth in the western Weddell–Scotia confluence. Marine Ecology Progress Series 366, 15–29.

Hewes, C.D., Reiss, C.S., Holm-Hansen, O., 2009. A quantitative analysis of sources for summertime phytoplankton variability over 18 years in the South Shetland Islands (Antarctica). Deep-Sea Research Part I 56, 1230–1241.

Holding, J.M., Duarte, C.M., Arrieta, J.M., Coello, A., Wassmann, P., Agustí, S., 2011. Temperature thresholds for Arctic plankton community metabolism: an experimental assessment. Biogeosciences Discussions 8, 11285–11309.

Holm-Hansen, O., Mitchell, B.G., 1991. Spatial and temporal distribution of phytoplankton and primary production in the western Bransfield Strait region. Deep Sea Research 38, 961–980.

Holm-Hansen, O., Kahru, M., Hewes, C.D., 2005. Deep chlorophyll a maxima (DCMs) in pelagic Antarctic waters. II. Relation to bathymetric features and dissolved iron concentrations. Marine Ecology Progress Series 297, 71–81.

Hopkinson, B.M., Mitchell, B.G., Reynolds, R.A., Wang, H., Selph, K.E., Measures, C.L., Hewes, C.D., Holm-Hansen, O., Barbeau, K.A., 2007. Iron limitation across Chlorophyll gradients in the southern Drake Passage: phytoplankton responses to iron addition and photosynthetic indicators of iron stress. Limnology and Oceanography 52, 2540–2554.

Howard, K.L., Yoder, J.A., 1997. Contribution of the subtropical oceans to global primary production. In: Liu, C.-T. (Ed.), Proceedings of COSPAR Colloquium on Space Remote Sensing of Subtropical Oceans, Taiwan. Space Remote Sensing of Subtropical Oceans. COSPAR Colloquia Series, vol. 8. Pergamon, New York, pp. 157–168.

Huang, K., Ducklow, H., Vernet, M., Casar, N., Bender, M.L., 2012. Export production and its regulating factors in the Western Antarctic Peninsula region of the Southern Ocean. Global Biogeochemical Cycles 19. http://dx.doi.org/10.1029/2010GB004028.

Irwin, A.J., Finkel, Z.V., Schofield, O.M.E., Falkowski, P., 2006. Scaling-up from nutrient physiology to the size-structure of phytoplankton communities. Journal of Plankton Research 28, 459–471.

Kara, A.B., Rochford, P.A., Hurlburt, H.E., 2000. An optimal definition for ocean mixed layer depth. Journal of Geophysical Research 105, 16803–16821.

Lee, S.H., Kim, B.K., Yun, M.S., Joo, H., Yang, E.J., Kim, Y.N., Shin, H.C., Lee, S., 2012. Spatial distribution of phytoplankton productivity in the Amundsen Sea, Antarctica. Polar Biology. http://dx.doi.org/10.1007/s00300-012-1220-5.

Li, W.K.W., Maestrini, S.Y., 1993. Measurement of primary production from the molecular to the global scale. ICES Marine Science Symposia 197, 1–2.

López-Urrutia, A., 2008. The metabolic theory of ecology and algal bloom formation. Limnology and Oceanography 53, 2046–2047.

López-Urrutia, A., San Martín, E., Harris, R.P., Irigoien, X., 2006. Scaling the metabolic balance of the oceans. Proceedings of the National Academy of Sciences of the United States of America 103, 8739–8744.

Lorenzo, L.M., Arbones, B., Figueiras, F.G., Tilstone, G.H., Figueroa, F.L., 2002. Photosynthesis, primary production and phytoplankton growth rates in Gerlache and Bransfield Straits during austral summer: cruise FRUELA 95. Deep-Sea Research Part II 49, 707–721.

MacIntyre, H.L., Kana, T.M., Anning, T., Geider, R.J., 2002. Photoacclimation of photosynthesis irradiance response curves and photosynthetic pigments in microalgae and cyanobacteria. Journal of Phycology 38, 17–38.
Marra, J., Ho, C., Trees, C., 2003. An alternative algorithm for the calculation of primary productivity from remote sensing data. LDEO Technical Report #LDEO-2003-1.
Martin, J.H., 1990. Glacial-interglacial CO_2 change: the iron hypothesis. Paleoceanography 5, 1–13.
Menden-Deuer, S., Lessard, E.J., 2000. Carbon to volume relationships for dinoflagellates, diatoms, and other protist plankton. Limnology and Oceanography 45, 569–579.
Milutinović, S., Bertino, L., 2011. Assessment and propagation of uncertainties in input terms through an ocean-color-based model of primary productivity. Remote Sensing of Environment 115, 1906–1917.
Moloney, C.L., Field, J.G., 1989. General allometric equations for rates of nutrient uptake, ingestion, and respiration in plankton organisms. Limnology and Oceanography 35, 1290–1299.
Moore, J.K., Abbott, M.R., 2000. Phytoplankton chlorophyll distributions and primary production in the Southern Ocean. Journal of Geophysical Research 105, 28709–28722.
Rintoul, S.R., Sparrow, M.D., Meredith, M., Wadley, V., Speer, K., Hoffman, E., Summerhayes, C.P., Urban, E., Bellerby, R., 2012. The Southern Ocean Observing System: Initial Science and Implementation Strategy. SCAR, Cambridge.
Ross, O.N., Geider, R.J., Piera, J., 2011. Modelling the effect of vertical mixing on bottle incubations for determination in situ phytoplankton dynamics. II. Primary production. Marine Ecology Progress Series 435, 33–45.
Sakshaug, E., Andresen, K., Kiefer, D.A., 1989. A steady state description of growth and light absorption in the marine planktonic diatom *Skeletonema costatum*. Limnology and Oceanography 34, 198–205.
Sangrà, P., Gordo, C., Hernádez-Arencibia, M., Marrero-Díaz, A., Rodríguez-Santana, A., Stegner, A., Martínez-Marrero, A., Pelegrí, J.L., Pichon, T., 2011. The Bransfield current system. Deep-Sea Research Part I 58, 390–402.
Sangrà, P., et al., 2012. Observations on phytoplankton distribution/size structure modulation by turbulence/dynamical stability and ageostrophic secondary circulation (ASC) in a no nutrient limited environment (Antarctica). Presented at the 2nd International Workshop, Nonlinear Processes in Oceanic and Atmospheric Flows, Madrid, Spain.
Sarmiento, J.L., Gruber, N., Brzezinski, M.A., Dunne, J.P., 2004. High-latitude controls of thermoclines nutrients and low latitude biological productivity. Nature 427, 56–60.
Shang, S.L., Behrenfeld, M.J., Lee, Z.P., O'Malley, R.T., Wei, G.M., Li, Y.H., Westberry, T., 2010. Comparison of primary productivity models in the Southern Ocean-preliminary results. Proc. SPIE 7678. http://dx.doi.org/10.1117/12.853631.
Smayda, T.J., 1997. Harmful algal blooms: their ecophysiology and general relevance to phytoplankton blooms in the sea. Limnology and Oceanography 42, 1137–1153.
Smith Jr., W.O., Gordon, L.I., 1997. Hyperproductivity of the Ross Sea (Antarctica) polynya during austral spring. Geophysical Research Letters 24, 233–236.
Smith Jr., W.O., Marra, J., Hiscock, M.R., Barber, R.T., 2000. The seasonal cycle of phytoplankton biomass and primary productivity in the Ross Sea, Antarctica. Deep-Sea Research Part II 47, 3119–3140.
Teira, E., Mouriño-Carballido, B., Martínez-García, S., Sobrino, C., Ameneiro, J., Hernández-León, S., Vázquez, E., 2012. Controls of primary production and bacterial carbon metabolism around South Shetland Islands. Deep-Sea Research Part I 69, 70–81.
Ting, K.C., Giacomelli, G.A., 1987. Availability of solar photosynthetically active radiation. Transactions of the ASABE 30, 1453–1457.
UNESCO, 1994. Protocols for the Joint Global Ocean Flux Study (JGOFS) core measurements. IOC Manuals and Guides. : , 29. UNESCO, Paris 97–100.
Varela, M., Fernández, E., Serret, P., 2002. Size-fractionated phytoplankton biomass and primary production in the Gerlache and south Bransfield straits (Antarctic Peninsula) in Austral summer 1995–1996. Deep-Sea Research Part II 49, 749–768.
Vernet, M., Smith, R.C., 2007. Measuring and modelling primary production in marine pelagic ecosystems. In: Fahey, T.J., Knapp, A.K. (Eds.), Principles and Standards for Measuring Primary Production. Oxford University Press, New York, pp. 142–174.
Vernet, M., Kozlowski, W., Yarmey, L.R., Lowe, A.T., Ross, R.M., Quetin, L.B., Fritsen, C.H., 2012. Primary production throughout austral fall during a time decreasing day length in the western Antarctic Peninsula. Marine Ecology Progress Series 452, 45–61.
Westberry, T., Behrenfeld, M.J., Siegel, D.A., Boss, E., 2008. Carbon-based primary productivity modeling with vertically resolved photoacclimation. Global Biogeochemical Cycles 22. http://dx.doi.org/10.1029/2007GB003078.